STUDY OF HEAT- AND MASS-TRANSFER CHARACTERISTICS IN THE SYMMETRY PLANES OF BODIES OF DIFFERENT SHAPES

V. I. Zinchenko and E. N. Putyatina

UDC 532.526.4

Results are presented from comparative studies of heat- and mass-transfer characteristics in flows about bodies of different shapes at angles of attack.

Several studies [1-3] have investigated characteristics of a supersonic three-dimensional laminar boundary layer near the symmetry planes of bodies of different shape. At the same time, it is interesting to analyze the effect of the geometry of the body, angles of attack, and gas injection from the surface on the heat- and mass-transfer characteristics for Reynolds numbers corresponding to different flow regimes in the boundary layer.

We will examine a three-dimensional flow having a symmetry plane. Let F(x, y, z) = 0 be the equation of the surface of a body in the flow in a Cartesian coordinate system xyz connected with the stagnation point of the flow. The velocity vector v_∞ is directed along the x axis. We will change over to a cylindrical coordinate system on the surface of the body $x = x$, $y = r_w(x, \psi)\sin\psi$, $z = r_w(x, \psi)\cos\psi$, where the angle ψ is reckoned from the symmetry plane y = 0 from the exposed or leeward side; r_w is the distance from the x axis to a point on the surface. The coordinate lines on the body are connected with sections of the surface by the planes x = const, ψ = const. The coordinate n is directed perpendicular to the surface. The components of the matrix tensor on the surface for the given coordinate system have the form:

$$g_{11} = g_{xx} = 1 + \left(\frac{\partial r_w}{\partial x}\right)^2,\quad g_{12} = g_{x\psi} = \frac{\partial r_w}{\partial x}\frac{\partial r_w}{\partial \psi},\quad g_{22} = g_{\psi\psi} = r_w^2 + \left(\frac{\partial r_w}{\partial \psi}\right)^2.$$

In the neighborhood of the symmetry plane, the expansion in the coordinate ψ for the sought functions and the coefficients of the system of equations of the three-dimensional boundary layer can be written

$$f = f^0 + f^1\psi^2 + \ldots,\quad f = \rho,\ p,\ u,\ v,\ H,\ T,\ r_w,\ w = w^0\psi + \ldots \tag{1}$$

Using an expansion of the components of the matrix tensor, allowing for (1), and using the general system of equations in [4] with allowance for the assumption of isotropy of the eddy viscosity coefficient, we can write the following system of equations of the three-dimensional boundary layer near the symmetry plane (the zero indices are omitted). The system is accurate to within small terms of the second order $0(\psi^2)$

$$\frac{\partial}{\partial x}(\rho u\sqrt{g_{22}}) + \rho w\sqrt{g_{11}} + \frac{\partial}{\partial n}(\rho v\sqrt{g_{11}g_{22}}) = 0, \tag{2}$$

$$\rho\left(\frac{u}{\sqrt{g_{11}}}\frac{\partial u}{\partial x} + v\frac{\partial u}{\partial n}\right) = -\frac{1}{\sqrt{g_{11}}}\frac{dp_e^0}{dx} + \frac{\partial}{\partial n}\left(\mu_\Sigma\frac{\partial u}{\partial n}\right), \tag{3}$$

$$\rho\left(\frac{u}{\sqrt{g_{11}}}\frac{\partial w}{\partial x} + \frac{w^2}{\sqrt{g_{22}}} + v\frac{\partial w}{\partial n} + B_1u^2 + B_3uw\right) = \frac{2r_w^1}{r_w^0}\frac{1}{g_{11}}\frac{dr_w^0}{dx}\frac{dp_e^0}{dx} - \frac{2p_e^1}{r_w^0} + \frac{\partial}{\partial n}\left(\mu_\Sigma\frac{\partial w}{\partial n}\right), \tag{4}$$

$$\rho\left(\frac{u}{\sqrt{g_{11}}}\frac{\partial H}{\partial x} + v\frac{\partial H}{\partial n}\right) = \frac{\partial}{\partial n}\left\{\frac{\mu_\Sigma}{\mathrm{Pr}_\Sigma}\left[\frac{\partial H}{\partial n} + (\mathrm{Pr}_\Sigma - 1)\frac{\partial}{\partial n}\left(\frac{u^2}{2}\right)\right]\right\}, \tag{5}$$

Tomsk State University. Translated from Inzhenerno-Fizicheskii Zhurnal, Vol. 50, No. 1, pp. 5-14, January, 1985. Original article submitted October 22, 1984.

0022-0841/86/5001-0001 $12.50

$$p = \rho h \frac{(\gamma - 1)}{\gamma}. \tag{6}$$

The value of B_1 and B_3 in (4) were determined near the symmetry plane with allowance for (1) from general expressions for B_i presented in [1].

Now changing over to the dimensionless arc length $ds = \frac{\sqrt{g_{11}^0}}{R_N} dx$ and using Dorodnitsin–Lees variables s, $\xi = \frac{u_e^0 r_w^0}{N} \int_0^n \rho dn$, $N = \left(2R_N \int_0^s \rho_e^0 \mu_e^0 u_e^0 (r_w^0)^2 ds\right)^{1/2}$, after introducing the stream functions f and φ near the symmetry plane, we obtain the following system:

$$\frac{\partial}{\partial \zeta}\left(l \frac{\partial^2 f}{\partial \zeta^2}\right) + (f + \alpha_2 \varphi) \frac{\partial^2 f}{\partial \zeta^2} = \alpha_1 \left(\frac{\partial f}{\partial \zeta} \frac{\partial^2 f}{\partial s \partial \zeta} - \frac{\partial f}{\partial s} \frac{\partial^2 f}{\partial \zeta^2}\right) + \beta_1 \left[\left(\frac{\partial f}{\partial \zeta}\right)^2 - \frac{\rho_e}{\rho}\right], \tag{7}$$

$$\frac{\partial}{\partial \zeta}\left(l \frac{\partial^2 \varphi}{\partial \zeta^2}\right) + (f + \alpha_2 \varphi) \frac{\partial^2 \varphi}{\partial \zeta^2} = \alpha_1 \left(\frac{\partial f}{\partial \zeta} \frac{\partial^2 \varphi}{\partial s \partial \zeta} - \frac{\partial f}{\partial s} \frac{\partial^2 \varphi}{\partial \zeta^2}\right) +$$
$$+ \beta_2 \left[\left(\frac{\partial \varphi}{\partial \zeta}\right)^2 - \frac{\rho_e}{\rho}\right] + \beta_3 \left[\left(\frac{\partial f}{\partial \zeta}\right)^2 - \frac{\rho_e}{\rho}\right] + \beta_4 \left[\frac{\partial f}{\partial \zeta} \frac{\partial \varphi}{\partial \zeta} - \frac{\rho_e}{\rho}\right], \tag{8}$$

$$\frac{\partial}{\partial \zeta}\left\{\frac{l}{\mathrm{Pr}_\Sigma} \frac{\partial g}{\partial \zeta} + \frac{u_e^2}{2H_e} l \left(1 - \frac{1}{\mathrm{Pr}_\Sigma}\right) \frac{\partial}{\partial \zeta}\left[\left(\frac{\partial f}{\partial \zeta}\right)^2\right]\right\} + (f + \alpha_2 \varphi) \frac{\partial g}{\partial \zeta} = \alpha_1 \left(\frac{\partial f}{\partial \zeta} \frac{\partial g}{\partial s} - \frac{\partial f}{\partial s} \frac{\partial g}{\partial \zeta}\right). \tag{9}$$

With allowance for injection along the normal to the surface, we write the boundary conditions as

$$\frac{\partial f}{\partial \zeta}(\infty, s) = 1, \quad \frac{\partial \varphi}{\partial \zeta}(\infty, s) = 1, \quad g(\infty, s) = 1,$$
$$\frac{\partial f}{\partial \zeta}(0, s) = 0, \quad \frac{\partial \varphi}{\partial \zeta}(0, s) = 0, \quad f(0, s) = f_w = \tag{10}$$
$$= \int_0^s (\rho \overline{v})_w \frac{r_w^0}{R_N} ds \Big/ \left[2 \int_0^s \frac{\rho_e^0}{\rho_{e0}} \frac{\mu_e^0}{\mu_{e0}} \frac{u_e^0}{v_m} \left(\frac{r_w^0}{R_N}\right)^2 ds\right]^{0,5},$$

$$\varphi(0, s) = \varphi_w = 0, \quad g(0, s) = g_w. \tag{11}$$

Here

$$\alpha_1 = \frac{2 \int_0^s \rho_e^0 \mu_e^0 u_e^0 (r_w^0)^2 ds}{\rho_e^0 \mu_e^0 u_e^0 (r_w^0)^2}, \quad \alpha_2 = \beta_2 = \alpha_1 \frac{w_e^0}{u_e^0} \frac{R_N}{r_w^0},$$

$$\beta_1 = \frac{\alpha_1}{u_e^0} \frac{du_e^0}{ds}, \quad \beta_3 = \alpha_1 \frac{u_e^0}{w_e^0} R_N B_1, \quad \beta_4 = \alpha_1 \left[\frac{1}{w_e^0} \frac{dw_e^0}{ds} + B_3^0 R_N\right],$$

$$R_N B_1^0 = \frac{2}{R_N} \frac{r_w^1}{r_w^0} \frac{d^2 r_w^0}{ds^2}, \quad R_N B_3^0 = \frac{1}{r_w^0} \frac{dr_w^0}{ds}.$$

We used the two-layer model of a turbulent boundary layer in [5] to describe three-dimensional turbulent flow. The eddy viscosity coefficient in the internal region was determined from the Prandtl formulas with the Van-Dreist–Sebechy damping factor, accounting for the effect of the pressure gradient on injection. This formula, used earlier to calculate two-dimensional flows, was extended to the case of a three-dimensional boundary layer; near the symmetry plane it has the form

$$\varepsilon = 0.16\rho n^2 \left\{1 - \exp\left(-\frac{n}{A}\right)\right\}^2 \frac{\partial u}{\partial n},$$

$$A = 26\nu \sqrt{\frac{\rho}{\tau_w}} \left\{\frac{\bar{p}}{\bar{v}_w}[1 - \exp(11.8\bar{v}_w)] + \exp(11.8\bar{v}_w)\right\}^{-1/2}, \tag{12}$$

$$\bar{p} = \frac{\nu u_e}{(\tau_w/\rho)^{3/2}} \frac{1}{R_N} \frac{du_e}{ds}, \quad \bar{v}_w = \frac{v_w}{(\tau_w/\rho)^{1/2}},$$

$$\tau_w = \mu_w \left.\frac{\partial u}{\partial n}\right|_w, \quad \nu = \frac{\mu}{\rho}.$$

In the external region, the eddy viscosity coefficient was calculated from the Clauser formula

$$\varepsilon = 0.0168\rho \left[1 + 5.5\left(\frac{n}{\delta}\right)^6\right]^{-1} \int_0^\infty (u_e - u)\, dn. \tag{13}$$

The boundary between the internal and external regions was determined from the condition of equality of coefficients (12) and (13).

The flow in the transitional region was calculated from the formula

$$\mu_\Sigma = \mu + \Gamma\varepsilon, \quad l = \frac{\rho\mu}{\rho_e\mu_e} + \Gamma\frac{\rho\varepsilon}{\rho_e\mu_e}, \quad \mathrm{Pr}_\Sigma = \frac{(\mu + \Gamma\varepsilon)\,\mathrm{Pr}\cdot\mathrm{Pr}_T}{\mu\mathrm{Pr}_T + \Gamma\varepsilon\mathrm{Pr}}, \tag{14}$$

where Γ is the coefficient of longitudinal compressibility proposed for the case of axisymmetric flow about blunt bodies and extended to the case of three-dimensional flow near symmetry planes [6]:

$$\Gamma = 1 - \exp\left\{-\Phi r_w^0 R_N^2 \left[\int_{s_n}^{s} (r_w^0)^{-1} ds\right]\left[\int_{s_n}^{s} u_e^{-1} ds\right]\right\},$$

$$\Phi = \frac{3u_e^3}{(Bv_e)^2}\mathrm{Re}_n^{-1,34}; \quad B = 60 + 4.68\mathrm{M}_n^{1,92}. \tag{15}$$

The coordinate of the point of loss of stability S_n, which corresponds to the beginning of the transitional flow region, was determined from the critical value of the Reynolds number:

$$\mathrm{Re}^{**} = \frac{u_e\rho_e\delta^{**}}{\mu_e} = 200, \quad \delta^{**} = \int_0^\infty \frac{\rho}{\rho_e}\frac{u}{u_e}\left(1 - \frac{u}{u_e}\right) dn. \tag{16}$$

For the laminar flow regime, $\Gamma = 0$. For the turbulent regime, $\Gamma = 1$.

The pressure distribution on the external boundary was prescribed from the Newton formula $p_e/p_{e0} = \cos^2\theta = \left(\frac{\gamma_{n\infty}}{v_\infty}\right)^2$, where θ is the angle between the normal to the surface at the stagnation point and the normal at the running point on the surface. In the coordinate system being used,

$$p_e/p_{e0} = \frac{r_w^2\left(\frac{\partial r_w}{\partial x}\right)^2}{r_w^2 + \left(\frac{\partial r_w}{\partial\psi}\right)^2 + r_w^2\left(\frac{\partial r_w}{\partial x}\right)^2} \tag{17}$$

and with allowance for (1), we can write an expansion for the relative pressure near the symmetry plane.

With a known pressure distribution, we find the values on the external boundary of the boundary layer from the relations

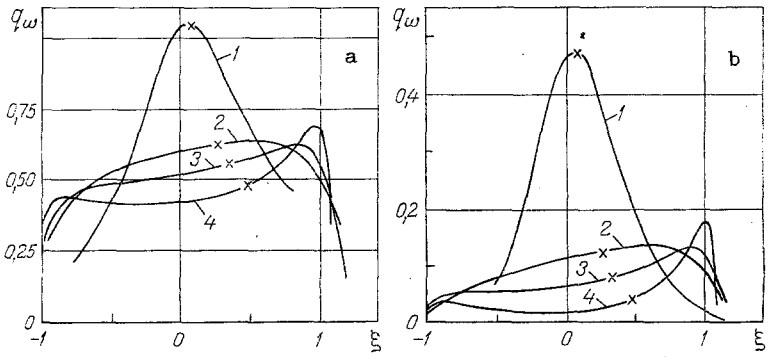

Fig. 1. Distribution of the dimensionless heat flux along the symmetry plane of ellipsoids of revolution: 1) k = 0.5, 2) 1.5, 3) 2, 4) 3.07; $g_w = 0.05$; a) $(\overline{\rho v})_w$ = 0, b) 1.

$$\frac{(u_e^0)^2}{v_m} = 1 - \left(\frac{p_e^0}{p_{e0}}\right)^{\frac{\gamma-1}{\gamma}}, \quad H_e = H_{e0}, \quad \frac{h_e}{H_{e0}} = \left(\frac{p_e^0}{p_{e0}}\right)^{\frac{\gamma-1}{\gamma}}. \tag{18}$$

To determine w_e^0, we need to integrate the following equation:

$$\rho_e^0\left[u_e^0\frac{dw_e^0}{ds} + \frac{(w_e^0)^2}{r_w^0}R_N + R_N B_1^0 (u_e^0)^2 + R_N B_3^0 u_e^0 w_e^0\right] = 2\frac{r_w^1}{r_w^0 R_N}\frac{dr_w^0}{ds}\frac{dp_e^0}{ds} - \frac{2p_e^1}{r_w^0}R_N. \tag{19}$$

The initial conditions for the initial system (7)-(9) can be obtained from the solution in the neighborhood of the stagnation point. Employing an expansion of the functions in the neighborhood of this point:

$$\psi = \psi_0 + \psi_1 s + \ldots \quad \left(\psi = \frac{\partial f}{\partial \zeta},\ \frac{\partial \varphi}{\partial \zeta},\ g,\ f,\ \varphi,\ \rho\right),$$
$$p_e/p_{e0} = 1 + p_1^0 s^2 + p_1^1 s^2\psi^2,\ r_w^0 = s + 0(s^3), \tag{20}$$
$$w_e^0 = \left.\frac{dw_e^0}{ds}\right|_0 s + \ldots,\ u_e^0 = \left.\frac{du_e^0}{ds}\right|_0 s + \ldots,\ 2\frac{r_w^1}{r_w^0} = 1 - \frac{R_1(0)}{R_2(0)},$$

where $R_1(0)$ and $R_2(0)$ are the principal radii of curvature at the critical point and R_1 corresponds to the lines in the symmetry plane, we can use (7)-(9) to obtain a system of ordinary differential equations with allowance for the fact that $\alpha_1(0) = \beta_3(0) = 0$, $\alpha_2(0) = \beta_2(0) = R_1(0)/R_2(0) - 1$, $\beta_1(0) = 1/2$, $\beta_4(0) = 1$.

Boundary-value problem (7)-(11) was integrated numerically by the interactive-interpolational method in [7]. The method of calculation was similar to the method in [8]. Equation (19) was integrated by the Runge-Kutta method. We made test comparisons with numerical data from [3, 9] and analytical solutions [3] for the laminar regime.

In the numerical calculations we varied the shape of the bodies (we examined a second-order surface), the angles of attack, the temperature factor, and the rate of gas flow $(\rho v)_w(s)$ from the surface. In the numerical integration, Pr = 0.72, Pr_T = 1, and the molecular viscosity coefficient was determined either by a power law or by the Suzerlend formula.

Let us examine the results of solution of the problem with flow about ellipsoids of revolution at angles of attack for the laminar regime in the boundary layer. The equation of the surface in Cartesian coordinates (x_c, y_c, z_c) connected with the symmetry plane has the following dimensionless form: $kx_c^2 + y_c^2 + z_c^2 = 1$, where k is the ratio of the semiaxes. Figure 1 shows the dependence of $q_w = \lambda_w \left.\frac{\partial T}{\partial n}\right|_w \sqrt{\mathrm{Re}}/v_m\rho_{e0}h_{e0}$ on ξ for solids of revolution with different values of k and an angle of attack $\alpha = 10°$. Here, ξ is the length of the arc reckoned from the symmetry axis of the body. The points denote the value of q_w at the stagnation point. In the calculation, we used a power law for μ with an exponent of 0.5.

It follows from the figure that an increase in k is accompanied by a substantial decrease in heat flux at the critical point $q_w(0)$, which is connected with an increase in the radius of curvature $R_1(0)$. We should point out the good agreement between the heat flux referred to its value in the case of axisymmetric flow and the values calculated from the analytical formula [3] $q_w(0)/q_w(0, \alpha=0)=\sqrt{\frac{1}{2}\left(1+\frac{R_1(0)}{R_2(0)}\right)}$. For prolate spheroids in the case of small values of k (curve 1), there is a monotonic decrease in heat flux going away from the critical point along the symmetry plane on both the exposed and leeward side. In the case $k \geqslant 1.5$, which corresponds to a monotinic increase in the curvature of the generatrix going away from the symmetry axis, the heat-flux maximum is shifted from the critical point on the exposed side to the region where the curvature of the contour and the velocity gradients of the external flow are maximal; on the leeward side, the flux q_w changes much less. Meanwhile, a second maximum considerably smaller than the first maximum is reached in the region of maximum curvature for k = 3.07.

It should be noted that the relative heat fluxes $q_w(s)/q_w(0)$ for the front part of the blunt body agree within 5% with data calculated from the analytical formula in [3].

It follows from comparison of Fig. 1a and Fig. 1b that a constant and identical rate of gas flow from the surface leads to a decrease in heat flux. Meanwhile, the maximum heat flux decreases considerably more for oblate spheroids than for prolate spheroids. As in the case of axisymmetric flow [8], this is connected with an increase in values of the stream function f_w as the body becomes blunter.

Figure 2 shows the effect of the angle of attack on the heat flux in flow about ellipsoids with a ratio of semiaxes k equal to 0.5 and 3.07. The values of the initial parameters agree with the corresponding values for Fig. 1. The curves in Fig. 2a correspond to flow along a nonpermeable surface, while the curves in Fig. 2b correspond to flow with $(\overline{\rho v})_w = 1$. An increase in the angle of attack is accompanied by an increase in the heat-flux maximum on the exposed side of the ellipsoid with k = 3.07 (the increase is by a factor of 1.7 for the case $\alpha = 30°$ compared to the case $\alpha = 5°$ (Fig. 2a)). The maximum heat flux decreases on the leeward side, but the change in the position of the maximum is small. It can be seen from the figure that an increase in the angle of attack is accompanied by a shift of the critical point toward the region of maximum curvature of the generatrix of the body. In this case, there is an increase in the gradients of the quantities on the external boundary of the boundary layer and a decrease in the thickness of the latter, which in turn causes a substantial increase in heat flux on the exposed side and on part of the leeward side. For prolate spheroids (k = 0.5), an increase in the angle of attack is accompanied by a decrease in the curvature of the generatrix at the critical point, which in turn leads to a decrease in the heat fluxes. Meanwhile, the maximum heat flux is seen at a point shifted from the critical point along the leeward side of the body (curves 5 and 6, Fig. 2).

For spheroids with k = 0.5, we should note the satisfactory agreement of the results of calculation with the system of boundary-layer equations in an axisymmetric approximation (dashed curves in Fig. 2) and the data from numerical integration in the exact formulation. The error of the approximate approach decreases markedly with an increase in k, which is connected with an increase in the intensity of secondary flows.

It follows from Fig. 2b that in the presence of injection, the heat-flux maximum $q_w(s)$ is more pronounced (the maximum relative heat flux $q_w(s)/q_w(0)$ increases with an increase in $(\overline{\rho v})_w$). With a specified value of flow rate, max $q_w(s)/q_w(0)$ increases with an increase in the angle of attack, which leads for oblate spheroids to a decrease in the efficiency of pore cooling on this section. Thus, in the region of maximum heat fluxes in the case k = 3.07, q_w/q_{w0} = 0.2, 0.25, and 0.5 for α = 5, 10, and 30°, respectively (q_{w0} corresponds to an impermeable surface).

Analysis of the calculated results in the form of the dependence of q_w/q_{w0} on the relative rate of flow of injected gas $(\overline{\rho v})_w/\left(\frac{\alpha}{c_p}\right)_0$, $\left(\frac{\alpha}{c_p}\right)_0=\frac{q_{w0}}{(1-g_w)}$ leads to the curve shown in Fig. 3. Here, q_{w0}, $\left(\frac{\alpha}{c_p}\right)_0$ corresponds to the heat flux and heat-transfer coefficient in the absence of injection, while curve I corresponds to the linear relation

$$q_w/q_{w0}=1-\varkappa(\overline{\rho v})_w/\left(\frac{\alpha}{c_p}\right)_0,\quad \varkappa=0.57-0.61. \tag{21}$$

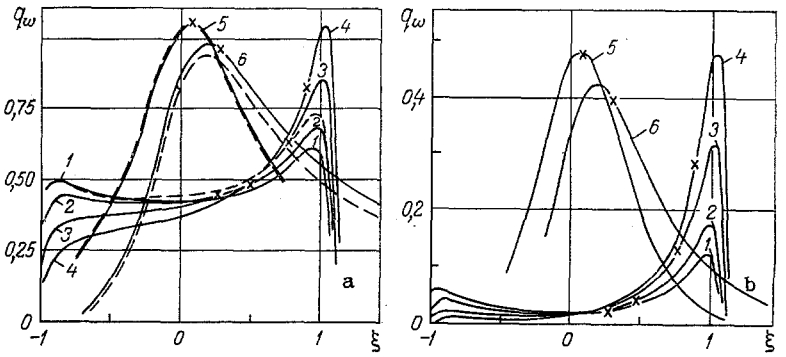

Fig. 2. Dependence of the heat flux on the longitudinal coordinate ξ: 1-4) k = 3.07; α = 5, 10, 20, 30°, respectively; 5, 6) k = 0.5; α = 10, 30° respectively.

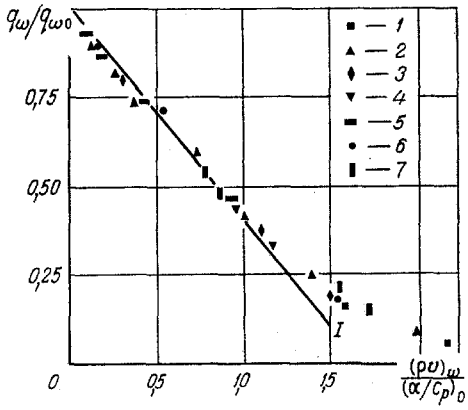

Fig. 3. Dependence of the ratio q_w/q_0 on the relative flow rate $\overline{(\rho v)_w}/(\alpha/c_p)_0$: 1-4) k = 3.07; α = 5, 10, 20, and 30°, respectively; 5-7) α = 10°, k = 0.5, 1.5, and 2 respectively.

The points denote the values of the ratio q_w/q_{w0} obtained for the ellipsoids with different angles of attack in the region from the critical point to the values of s on the lateral surface corresponding to the maximum heat flux. It follows from the figure that Eq. (21) can be used for moderate injection near the symmetry plane in a fairly broad range of s beginning with the critical point.

$\frac{\partial\varphi}{\partial\zeta}$ On the leeward side, for several shapes beginning with a certain value of s, the profile across the boundary layer becomes nonmonotonic, while the component of the friction-stress vector $\mu\frac{\partial w}{\partial n}\Big|_w$ changes sign. To analyze the flow in this case, we projected the stress vector on the surface $\tau_w = \mu_w\frac{\partial u}{\partial n}\Big|_w \mathbf{i}_1 + \mu_w\frac{\partial w}{\partial n}\Big|_w \mathbf{i}_2$ in a direction in the tangent plane to the body and perpendicular to the symmetry plane:

$$\mu_w^0\frac{\partial w^0}{\partial n}\Big|_{w,N} = \mu_w^0\frac{\partial w^0}{\partial n}\Big|_w + \mu_w^0\frac{\partial u^0}{\partial n}\Big|_w\frac{dr_w^0}{dx}\frac{1}{\sqrt{g_{11}^0}}.$$

In this case, if $\mu_\omega^0\frac{\partial w^0}{\partial n}|_{w,N}$ changes sign and becomes negative, there is a shift in the flow direction in relation to the symmetry plane and, in accordance with the concept advanced in [10], the formation of a transverse eddy may lead to separation of the flow. It should be noted that, for these sections, the error of the analytical formulas for $q_w/q_w(0)$ [3] is significantly greater.

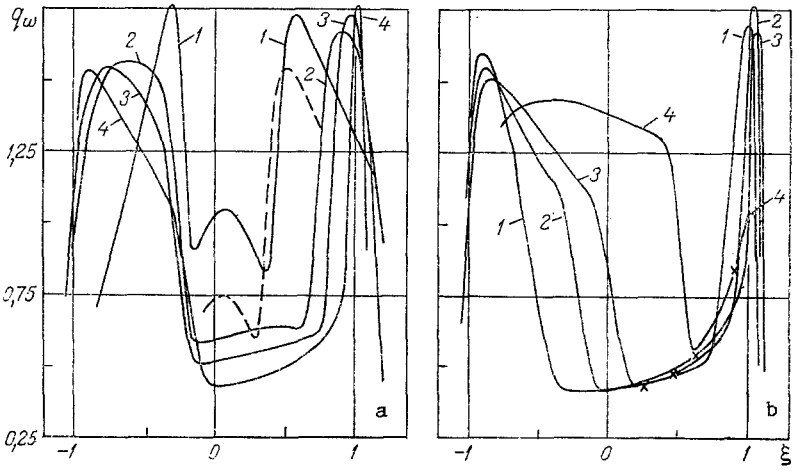

Fig. 4. Distribution of heat flux near the symmetry plane of an ellipsoid of revolution: a) $\alpha = 10°$, 1-4) $k = 0.5$; 1.5; 2) 3.07 respectively; b) $k = 3.07$, 1-4) $\alpha = 5$, 10, 15, 30°, respectively.

Let us examine flow for Reynolds numbers corresponding to laminar, transient, and turbulent flow regimes in the boundary layer. Figure 4 shows the dependence of q_w on ξ for different shapes of ellipsoids of revolution with flow at a specified angle of attack (Fig. 4a), as well as for $k = 3.07$ with different angles of attack (Fig. 4b). Here, $(\overline{\rho v})_w = 0$, $Re = 5.7 \cdot 10^6$. The remaining parameters are the same as in Fig. 1.

It follows from Fig. 4a that heat flux increases sharply in the transient and turbulent regions compared to the case of a laminar boundary layer (Fig. 1a). Meanwhile, on the exposed side for ellipsoids with $k \geqslant 2$, the region of maximum heat flux is shifted slightly downstream compared to the region of the maximum of $q_w(\xi)$ for laminar flow. It must also be noted that, in contrast to Fig. 1a, the values of maximum heat flux are similar for ellipsoids with different ratios of semiaxes. For the given flow regimes, in accordance with the specified pressure distribution, the heat flux is higher on the leeward side for oblate ellipsoids than on the exposed side. For prolate ellipsoids (curve 1), the nonmonotonic behavior of $q_w(\xi)$ is due to a shift in flow regimes. Due to the large pressure gradients along the generatrix, the maximum heat flux is somewhat greater on the leeward side than the value of $q_w(\xi)$ on the exposed side. It should be noted that, as in the case of axisymmetric flow, when Re increases the position and magnitude of the heat-flux maximum is independent of whether or not the transient region is taken into account.

To find the distribution $q_w(\xi)$, it is important to have a criterion to determine the point of loss of stability. Thus, we need additional information to refine (16) for the case of three-dimensional flow in the boundary layer.

It is evident from Fig. 4b that, in contrast to the case of laminar flow in the boundary layer, a change in the angle of attack has a slight effect on the magnitude and position of the heat-flux maximum. The increase in $q_w(\xi)$ on the leeward side is connected with the position of the point of loss of stability. Meanwhile (see Fig. 4b, curve 4), for large angles of attack, $q_w(\xi)$ in this flow region is significantly greater than the heat flux on the exposed side. This is connected with the fact that in this case $Re^{**} < 200$ on the exposed side, and laminar flow is realized in the boundary layer.

The calculations showed that in the case of a complex flow regime with gas injection into the boundary layer (see the dashed curve in Fig. 4a corresponding to flow about an ellipsoid with $k = 0.5$ at $(\overline{\rho v})_w = 0.5$), the flow becomes unstable and the point of loss of stability is shifted toward the stagnation point. Thus, for several values of s, heat flux with injection may be greater than the corresponding value of q_w for an impermeable wall.

Analysis of the numerical results showed that the linear relation $q_w/q_{w0} = f\left((\overline{\rho v})_w \Big/ \left(\frac{\alpha}{c_p}\right)_0\right)$ can also be used to evaluate heat flux in the region of developed turbulent flow on the exposed side where the maximum heat flux is realized for small values of the injection parameter $(\overline{\rho v})_w/(\alpha/c_p)_0 \leqslant 0.5$.

Thus, it follows from analysis of the results obtained that heat flow to the body can be reduced by using blunt shapes (oblate spheroids). This conclusion is valid in a limited range of the angle of attack, with laminar flow in the boundary layer.

When flow in the boundary layer is turbulent, the maximum local heat fluxes for bodies of different shapes are close in magnitude and change slightly with a change in the angle of attack $0 \leqslant \alpha \leqslant 15°$. For blunt bodies, the position of the region of maximum heat flux on the exposed side changes slightly for different flow regimes in the boundary layer and changes conservatively in relation to the angle of attack.

NOTATION

x, ψ, n, curvilinear coordinates connected with the surface of the body in the flow; f, φ, dimensionless stream functions; $f'_\xi = u/u_e$, $\varphi'_\xi = w/w_e$, dimensionless components of velocity; H, enthalpy; ρ, density; $g = H/H_{e0}$, dimensionless enthalpy; μ, λ, viscosity coefficient and thermal conductivity; Pr, $\mathrm{Re} = v_m \rho_{e0} R_N / \mu_{e0}$, $v_m = \sqrt{2H_{e0}}$, Prandtl and Reynolds numbers and maximum velocity; R_N, characteristic dimension of the body; $(\overline{\rho v})_w = (\rho v)_w \sqrt{\mathrm{Re}}/v_m \rho_{e0}$, dimensionless rate of flow of gas from the surface. Indices: e, e0, and w correspond to quantities on the external boundary of the boundary layer, on the external boundary at the stagnation point, and on the surface of the body.

LITERATURE CITED

1. Yu. D. Shevelev, Three-Dimensional Problems of Laminar Boundary Layer Theory [in Russian], Nauka, Moscow (1977).
2. S. I. Seliverstov, "Calculation of a laminar boundary layer on the spread line of the front surface of a segmented body in a supersonic gas flow," Izv. Akad. Nauk SSSR, Mekh. Zhidk. Gaza, No. 4, 109-114 (1968).
3. I. G. Brykina, E. A. Gershbein, and S. V. Peigin, "Laminar boundary layer in the symmetry planes of blunt bodies with angles of attack and injection or suction," Izv. Akad. Nauk SSSR, Mekh. Zhidk. Gaza, No. 5, 37-48 (1980).
4. V. A. Aleksin and Yu. D. Shevelov, "Three-dimensional boundary value problems on bi-elliptical bodies in a compressible-gas flow with an angle of attack," Izv. Akad. Nauk SSSR, Mekh. Zhidk. Gaza, No. 2, 39-47 (1983).
5. T. Sebechi, "Calculation of a three-dimensional boundary layer, An infinite cylinder with slip and a small secondary flow," Raket. Tekh. Kosmon., No. 6, 53-63 (1974).
6. N. P. Kolina and E. E. Solodkin, "Program in FORTRAN for numerical integration of the equations of a three-dimensional boundary layer on the spread line and on an infinite sliding cylinder," Tr. TsAGI, No. 2046 (1980).
7. A. M. Grishchin and V. N. Bertsun, "Iterative-interpolational method and the theory of splines," Dokl. Akad. Nauk SSSR, 214, No. 4, 751-754 (1974).
8. V. I. Zinchenko and E. N. Putyatina, "Study of heat and mass transfer in flow about bodies of different shapes with allowance for injection," Inzh.-Fiz. Zh., 45, No. 1, 11-21 (1983).
9. I. P. Morozov, "Laminar boundary layer on the spread line of ellipsoids of revolution," Izv. Akad. Nauk SSSR, Mekh. Zhidk. Gaza, No. 6, 50-53 (1968).
10. Young, "Laminar boundary layer near the frontal symmetry surface of an elongated spheroid," Raketn. Tekh. Kosmon., No. 7, 85-96 (1974).